Design Of Dual Active Bridge Converters For Electric Vehicles—Evaluating Modulation Schemes And Operating Frequencies

by Silpashree Sahu, Abinash Dash, Dipankar De, Harikrishnan A, and Varri Chandra Sekhar Pavan Kumar, IIT Bhubaneswar, Jatni, India and Alberto Castellazzi, Kyoto University of Advanced Sciences, Kyoto, Japan

Electric vehicles (EVs) are now becoming quite popular in modern cities in order to reduce dependency on fossil fuel. In green city initiatives and in the Made in India mission, the design, development and marketing of electric vehicles and their internal configurations are given high importance.[1,2] India aims to reach approximately 80% electrification of two- and three-wheelers, about 70% of commercial vehicles, around 40% of buses, and roughly 30% of private passenger cars by 2030.[3]

However, while EVs are seeing increased adoption, hybrid electric vehicles (HEVs) which combine an internal combustion engine (ICE) with an electrically driven power train, are also making their way to market. Among the different types of HEVs, the plug-in hybrid is one option.

Fig. 1 shows the configuration of a plug-in electric vehicle with an additional 48-V battery for electric steering along with the main high-voltage (HV) battery for driving the transmission system. The HV battery can be charged from the ac mains through a rectifier unit and it can be charged from an ICE-fed generator as well through the on-board power electronics converters.[4,5]

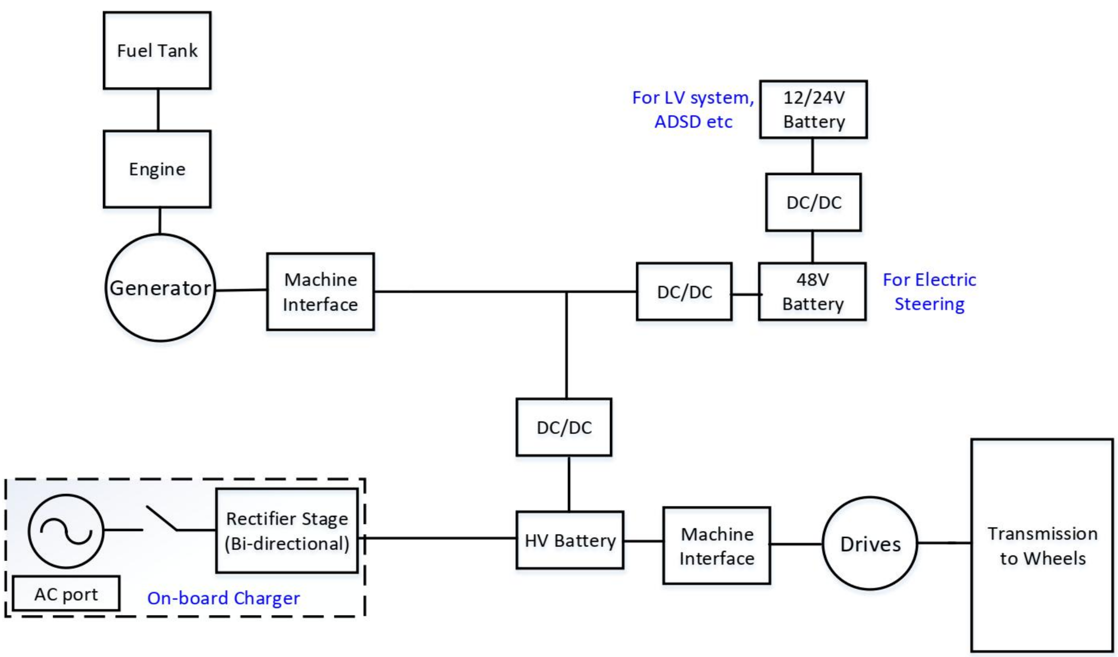

Fig. 1. Typical configuration for plug-in series hybrid electric vehicle.[2]

The most commonly used power converter configurations for such HEV and other EV systems are dual active bridge (DAB) to interface different voltage levels.[6,7] This article will first focus on the operating principle of dual active bridge as relates to the control method or modulation technique employed. The three different modulation methods—single-phase-shift, triple-phase-shift and extended-phase-shift control—are introduced with waveforms presented to illustrate how they determine switching of the two H-bridges.

From there, we proceed to explain the key elements of DAB converter design, presenting the equations required for determining the link inductance and transformer turns ratio, which are then used in determining the peak and RMS current ratings of the power switches. This is followed by a discussion of magnetic design, that is core selection and winding design for the transformer and inductor. Then, the equations needed to calculate the losses of the power switches and magnetics are presented.

With these last equations in hand, we can proceed to the study our team conducted on DAB converter losses as a function of modulation method at the two switching frequencies which represent the range of the specified converter's operation. Then, simulation results reveal the impact of the different modulation methods on switch stress and loss.

These are followed by experimental results for a prototyped converter at the two frequency extremes, and two power output levels. Measurements of switching waveforms and output voltage demonstrate actual performance under single-phase-shift control and thermal images reveal maximum temperature rises at the higher power level.

Operation Of Conventional Dual Active Bridge Converter

The basic structure of the DAB converter is shown in Fig. 2.

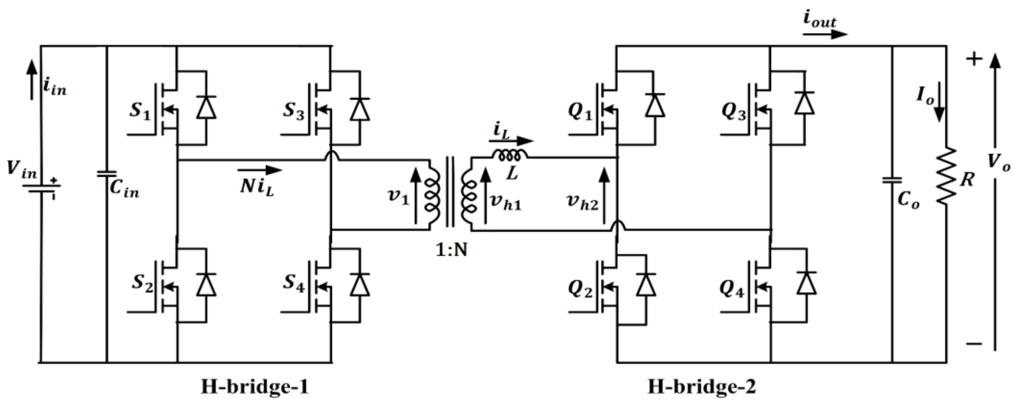

Fig. 2. Power circuit diagram of conventional dual active bridge (DAB) converter.

The most widely used control method for DAB is single-phase-shift (SPS) control,[8] where a single phase-shift (D_2) exists between H-bridge-1 and H-bridge-2. The power flow direction and magnitude can be controlled by adjusting the phase shift (D_2) between v_{h1} and v_{h2}.

The generalized modulation technique employed is triple phase-shift (TPS) control,[9,10] which incorporates not only an outer phase shift but also inner phase shifts within H-bridge-1 and H-bridge-2. Specifically, D_1 and D_3 represent the inner phase shifts of H-bridge 1 and H-bridge 2, respectively. Extended phase-shift (EPS) control[11] is a special case of TPS control where the inner phase shift occurs in only one H-bridge. The illustrative waveforms of SPS, TPS, and EPS control methods are shown in Fig. 3.

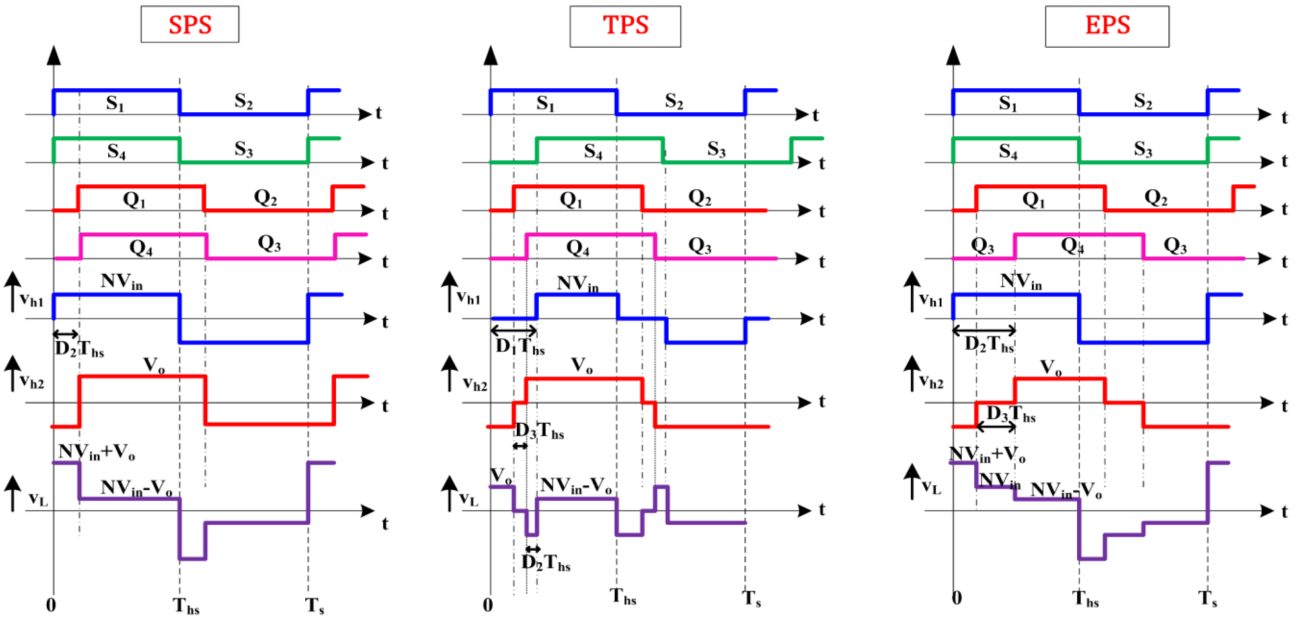

Fig. 3. Illustrative waveforms for the different modulation techniques.

Design Of Conventional Dual Active Bridge Converter

The design of the dual active bridge is carried out by selecting an appropriate link inductance and a turns ratio of the transformer. The specification of the converter is given in Table 1.

Table 1. Specification of DAB.

Attributes	DAB
Port-1 (V_{in})	40 to 75 V
Port-2 (V_o)	375 V
Rated power (P_o)	1 kW
Switching frequency (f)	20 to 50 kHz
L	90 to 225 μH
Turns ratio (N)	6

The variation of link current stress (peak value of i_L) with input voltage (V_{in}) at 1-kW load power is shown in Fig. 4. As observed from the figure, the link current stress attains its peak value at an input voltage of 40 V, identifying this as the worst-case operating condition for the converter. Therefore, the design and sizing of the link inductance must be conducted considering this scenario to guarantee optimal performance and ensure that the converter can withstand the maximum current stress without compromising reliability.

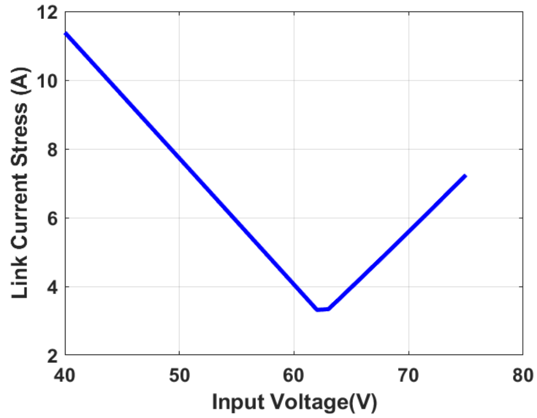

Fig. 4. Variation of link current stress with input voltage at 1-kW load.

Assuming the maximum power P_{max} transferred is 2.5 times the rated power, the link inductance (L) is calculated using the following expression.

$$L = \frac{NV_{in}V_o}{8fP_{max}} = \frac{6\times40\times375}{8\times20000\times2.5\times1000} = 225\ \mu H \qquad (1)$$

where N, V_{in}, V_o, f and P_{max} are the terms defined above.

The turns ratio is chosen as 6 assuming the nominal input voltage is 65 V ($N = \frac{375}{65} = 5.77 \approx 6$).

For the single-phase shift (SPS) modulation technique (see Fig. 4 again), the peak and RMS values of the link current are determined based on the corner point currents of the waveform. The different corner point current expressions are given below.

Voltage Conversion Ratio, $k = \frac{V_o}{NV_{in}}$ (2)

$$i_L(0) = -\frac{NV_{in}}{4fL}[1 + k(2D_2 - 1)] \qquad (3)$$

$$i_L(D_2T_{hs}) = \frac{NV_{in}}{4fL}[k + (2D_2 - 1)] \qquad (4)$$

where

$$D_2 = 0.5\left[1 - \sqrt{1 - \frac{8fLP_o}{NV_{in}V_o}}\right] \qquad (5)$$

$$i_L(T_{hs}) = -i_L(0) \qquad (6)$$

Now, let the peak value of link current be I_{pk}. Then for

$\boldsymbol{I_{pk}} = \boldsymbol{i_L}(D_2T_{hs})$ for k > 1 and $\boldsymbol{I_{pk}} = \boldsymbol{i_L}(T_{hs})$ for k < 1 (7)

The RMS value of the link current (I_{rms}) can be calculated from the link current waveform by utilizing the various corner point values.

$$I_{rms} = \sqrt{\frac{1}{3}[Di_L^2(0) + (D_2 - D)i_L^2(D_2T_{hs}) + (1 - D_2)\{i_L^2(T_{hs}) - i_L^2(D_2T_{hs})\}] + (1 - D_2)i_L^2(D_2T_{hs})} \quad (8)$$

where

$$D = D_2 - \frac{i_L(D_2T_{hs})}{mT_{hs}} \quad (9)$$

The m term is then defined as

$$m = \frac{NV_{in} + V_o}{L} \quad (10)$$

Subsequently, the RMS currents for the switches are derived from the link inductance RMS current. For H-bridge-2, the switch RMS current is denoted as I_{sw2}, and for H-bridge-1, it is denoted as I_{sw1}:

$$I_{sw2} = \frac{I_{rms}}{\sqrt{2}} \text{ and } I_{sw1} = \frac{NI_{rms}}{\sqrt{2}} \quad (11)$$

Blocking voltage ratings of H-bridge-1 and H-bridge-2 switches are V_{in} and V_o, respectively.

Magnetic Design

For a dual active bridge converter, the magnetic design plays an important role and the design depends on the configurations of the magnetic components.[12,13] The design steps for the high-frequency transformer and inductor are summarized as follows.

1. Calculate area product

Transformer: For a given specification of volt-ampere (VA), V_1, V_2, J (current density), B_m, k_w (winding factor), and f of a transformer, compute the area product ($A_{p(t)}$) of the desired core and select the smallest core from the available cores.

$$A_{p(t)} = \frac{VA}{2fk_wJB_m} \quad (12)$$

Inductor: To calculate the area product of an inductor ($A_{p(i)}$), it is necessary to know both the peak and RMS currents flowing through it.

$$A_{p(i)} = \frac{LI_{pk}I_{rms}}{k_wJB_m} \quad (13)$$

2. Select the smallest core from the core tables having an area product higher than that obtained in the above step.
3. Find the core area (A_c) and window area (A_w) of the selected core.
4. The no. of turns in the primary and secondary windings of the transformer is given below.

$$N_1 = \frac{V_1}{4fB_mA_c} \quad (14)$$

$$N_2 = NN_1 \quad (15)$$

The no. of turns in the winding of the inductor is given below.

$$N_i = \frac{LI_{pk}}{B_m A_c} \quad (16)$$

5. Compute the wire size and select a wire whose diameter is nearly two times the skin depth.

$$a_w = \frac{I}{J} \quad (17)$$

6. Calculate the number of parallel wires.

$$\boldsymbol{n} = \frac{\boldsymbol{a_w}}{\boldsymbol{a}} \quad (18)$$

where a is the cross-sectional area of the selected wire.

7. Find the bobbin size based on the number of cores used in the design. From the bobbin height, find the number of turns of n parallel wires in one layer.

$$N_l = \frac{h_{bobbin}}{n d_{we}} \quad (19)$$

where d_{we} is the diameter of the wire with enamel.

8. Find the number of layers in primary and secondary windings.

$$NL = \frac{N}{N_l} \quad (20)$$

Calculate the length (l) of a single parallel wire for both windings and find the dc resistance (R_{dc}) of a single parallel wire.

$$R_{dc} = \frac{\rho l}{a} \quad (21)$$

where ρ is the resistivity of the wire.

9. The dc winding resistance is given by

$$R_{wdc} = \frac{R_{dc}}{n} \quad (22)$$

10. From Dowell's equation,[13] the ac-to-dc winding resistance ratio for the solid-round-wire winding at the k^{th} harmonic frequency can be expressed as

$$F_{Rk} = \sqrt{k}A\left[\frac{sinh(2\sqrt{k}A)+sin(2\sqrt{k}A)}{cosh(2\sqrt{k}A)-cos(2\sqrt{k}A)} + \frac{2(NL^2-1)}{3}\frac{sinh(\sqrt{k}A)-sin(\sqrt{k}A)}{cosh(\sqrt{k}A)+cos(\sqrt{k}A)}\right] \quad (23)$$

$$A = \left(\frac{\pi}{4}\right)^{0.75}\frac{d_{woe}}{\delta}\sqrt{\eta} \quad (24)$$

where A is the effective diameter of the solid round wire winding, d_{woe} is the diameter of the bare conductor, δ is the skin depth of the conductor, and η is the ratio of d_{woe} to d_{we}.

11. The ac resistance of a winding for k^{th} harmonic frequency is

$$R_{wk} = F_{Rk} R_{wdc} \quad (25)$$

Loss Calculation

1. The switch conduction loss[13] is given by

$$P_{c(sw)} = I_{sw}^2 \, R_{ds(on)} \tag{26}$$

where I_{sw} and $R_{DS(ON)}$ are the RMS current and on-state resistance of the switch.

2. The switching loss of a switch is given by

$$P_{s(sw)} = \frac{1}{2} f V_{sw} I_{sw} (t_r + t_f) \tag{27}$$

where V_{sw} and I_{sw} are the voltage and current at the time of switching, respectively and t_r and t_f are the rise time and fall times, respectively.

3. The conduction loss of a transformer/inductor is given by

$$P_{c(t/i)} = \sum_{s=1}^{Z} (P_{dc,s} + P_{ac,s}) \tag{28}$$

where z is the number of windings, $P_{dc,s}$ and $P_{ac,s}$ are dc and ac power losses in the windings respectively.

4. The core loss of a transformer/inductor is given by

$$P_{core(t/i)} = \left[\sum_{k=1,3,5,\dots} k_1 f_k^{\alpha} B_{mk}^{\beta} \right] V_{core} \tag{29}$$

where k_1, α, and β are constants whose values depend on the core material. f_k, B_{mk} and V_{core} are k^{th} harmonic frequency, the maximum flux density of kth harmonic component and the volume of the core, respectively.

Comparative Study With Different Modulation Techniques

The performance of the dual active bridge converter is significantly dependent on the modulation strategy employed. In this section, a comparative study is presented with SPS, EPE and TPS modulation methods. The conventional DAB with SPS control is compared with DAB with TPS and EPS control in terms of different (semiconductor, transformer, inductor) losses. Table 2 presents the specifications of various semiconductor switches across a range of operating points for the three modulation techniques: SPS, TPS, and EPS.

Table 3 presents the conduction and switching losses for the semiconductor switches at a given operating point. It can be observed that the Set-1 switches exhibit lower conduction losses, attributed to their lower on-state resistance. In contrast, the Set-2 switches demonstrate reduced switching losses due to shorter rise and fall times.

It can be noted that for selection of switches Set-1 and Set-2 are purely for illustration purposes. A different and even better selection of switches can always be made from the available power semiconductor switches in the market.

The magnetic designs corresponding to the SPS, TPS, and EPS modulation techniques are summarized in Table 4, while the associated magnetic losses are detailed in Table 5. This comparison helps to select appropriate switching frequency, semiconductor switches and magnetic core for the converter.

Table 2. Switch selection.

Operating points (V_{in}, V_o, f_{sw})	Topology/ modulation techniques	Set-1 switches		Set-2 switches	
		H-bridge 1	H-bridge 2	H-bridge 1	H-bridge 2
40 to 75 V, 375 V, 20 to 50 kHz	DAB+SPS[8]	NTP6410ANG, 100 V, 76 A, 11 mΩ, 170 ns (t_r), 190 ns (t_f)	SCT10N120, 1200 V, 12 A, 500 mΩ, 120 ns(t_r), 17 ns (t_f)	IRFP260N,200 V, 50 A, 40 mΩ, 60 ns(t_r), 48 ns (t_f)	SCT2450KE,1200 V, 10 A,450 mΩ, 17 ns (t_r), 34 ns (t_f)
	DAB+TPS[9]	PSMN013-100YSEX,100 V, 58 A, 11 mΩ, 23 ns (t_r), 21 ns (t_f)	G3R350MT12D, 1200 V, 10 A,350 mΩ, 10 ns (t_r), 7 ns (t_f)	IRFP260N, 200 V, 50 A,40 mΩ, 60 ns(t_r), 48 ns (t_f)	SCT2450KE,1200 V, 10 A, 450 mΩ, 17 ns (t_r), 34 ns (t_f)
	DAB+EPS[10]	PSMN013-100YSEX, 100 V, 58 A, 11 mΩ, 23 ns (t_r), 21 ns (t_f)	G3R350MT12D, 1200 V, 10 A, 350 mΩ, 10 ns (t_r), 7 ns (t_f)	IRFP260N, 200 V, 50 A, 40 mΩ, 60 ns (t_r), 48 ns (t_f)	SCT2450KE, 1200 V, 10 A, 450 mΩ, 17 ns (t_r), 34 ns (t_f)

Table 3. Switch losses.

Topology/ modulation techniques	Operating points (V_{in}, f_{sw}) (P_o = 1 kW)	Losses of set-1 switches		Losses of set-2 switches	
		Conduction (W)	Switching (W)	Conduction (W)	Switching (W)
DAB+SPS[8]	40 V, 20 kHz	66.683	1.784	175.55	0.601
	75 V, 200 kHz	34.251	0.638	93.776	1.257
	40 V, 50 kHz	66.683	4.461	175.55	1.501
	75 V, 50 kHz	34.251	1.595	93.776	3.144
DAB+TPS[9]	40 V, 20 kHz	39.127	0.0227	106.581	0.086
	75 V, 20 kHz	16.844	0.0376	38.658	0.013
	40 V, 50 kHz	39.005	0.089	112.440	0.229
	75 V, 50 kHz	16.003	0.280	42.294	0.464
DAB+EPS[10]	40 V, 20 kHz	32.762	0.023	79.602	0.012
	75 V, 20 kHz	13.888	0.0425	32.252	0.019
	40 V, 50 kHz	32.127	0.021	78.856	0.052
	75 V, 50 kHz	13.094	0.084	32.241	0.132

Table 4. Magnetic design (wire -SWG 22, core material N27).

Operating frequency (f)	Topology/modulation techniques	Attributes	Transformer	Inductor
20 kHz	DAB+SPS[8]	A_p (mm^4)	365090	91609
		Core	E42/21/15	E42/21/15
		M	8	2
		Parallel wires	29 (primary), 5 (secondary)	5
50 kHz	DAB+SPS[8]	A_p (mm^4)	146030	36644
		Core	E36/18/11	E36/18/11
		M	8	2
		Parallel wires	29 (primary), 5 (secondary)	5
20 kHz	DAB+TPS[9]	A_p (mm^4)	284460	50887
		Core	E65/32/13	E42/21/9
		M	2	2
		Parallel wires	23 (primary), 4 (secondary)	4
50 kHz	DAB+TPS[9]	A_p (mm^4)	116870	20907
		Core	E42/21/20	E40/17/11
		M	2	2
		Parallel wires	23 (primary), 4 (secondary)	4
20 kHz	DAB+EPS[10]	A_p (mm^4)	251040	40136
		Core	E47/20/16	E36/6/18
		M	8	8
		Parallel wires	20 (primary), 3 (secondary)	3
50 kHz	DAB+EPS[10]	A_p (mm^4)	100410	16054
		Core	E40/17/11	E34/14/9
		M	8	2
		Parallel wires	20 (primary), 3 (secondary)	3

A_p = area product of the required core, M = no. of E-cores required.

Table 5. Power loss.

Topology/ modulation techniques	Operating points (V_{in}, f_{sw}) (P_o = 1 kW)	Semiconductor		Transformer		Inductor	
		Conduction loss (W)	Switching loss (W)	Conduction loss (W)	Core loss (W)	Conduction loss (W)	Core loss W)
DAB+SPS[8]	40 V, 20 kHz	66.683	1.784	12.559	6.217	5.445	2.657
	75 V, 20 kHz	34.251	0.638	11.997	8.998	5.016	2.801
	40 V, 50 kHz	66.683	4.461	13.153	11.055	5.947	4.332
	75 V, 50 kHz	34.251	1.595	12.968	13.581	5.694	4.565
DAB+TPS[9]	40 V, 20 kHz	39.127	0.023	10.013	4.308	5.033	2.082
	75 V, 20 kHz	16.844	0.037	9.638	6.821	4.976	2.115
	40 V, 50kHz	39.005	0.089	11.296	9.264	5.791	3.773
	75 V, 50 kHz	16.002	0.280	10.649	11.839	5.424	3.935
DAB+EPS[10]	40 V, 20 kHz	32.762	0.023	9.644	4.018	4.841	1.851
	75 V, 20 kHz	13.878	0.042	8.186	6.327	4.556	1.942
	40 V, 50 kHz	32.127	0.021	10.183	7.935	5.232	3.436
	75 V, 50 kHz	13.094	0.084	9.893	9.016	5.095	3.695

It can be observed that the efficiency of the converter significantly depends on the variation of the input voltages. The effects of this variation along with modulation method in terms of total loss (including semiconductor and magnetic losses) are summarized in Fig. 5.

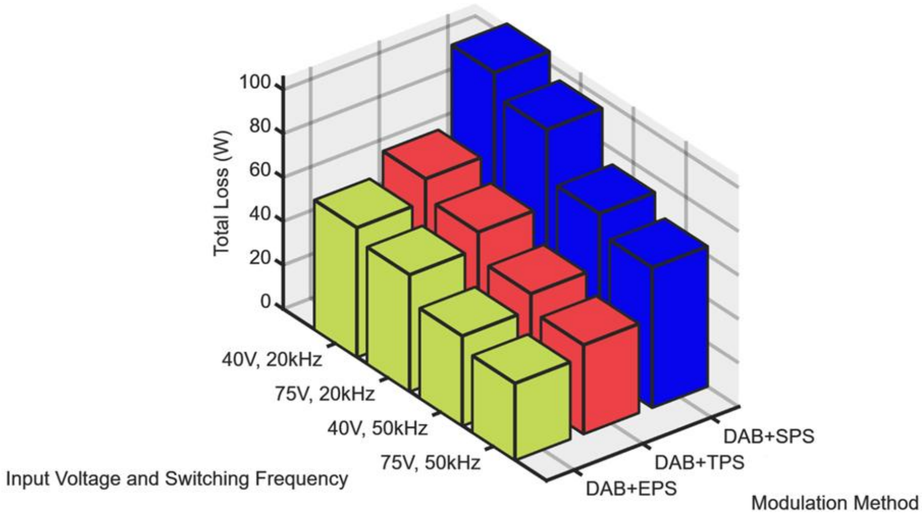

Fig. 5. Comparison of total loss at different operating points and with different modulation techniques: SPS [8], TPS [9] and EPS [10].

Simulation Results

Fig. 6 illustrates the simulation results for the DAB converter using SPS, TPS, and EPS control methods. The results indicate that the EPS control achieves the lowest peak link current, while the SPS control results in the highest peak value.

It can be clearly observed from the waveform that the peak-to-peak current in the ac link is lower with TPS and EPS modulation compared to that with SPS for the same power transfer. This results in reduced switch stress and reduced losses in the converter.

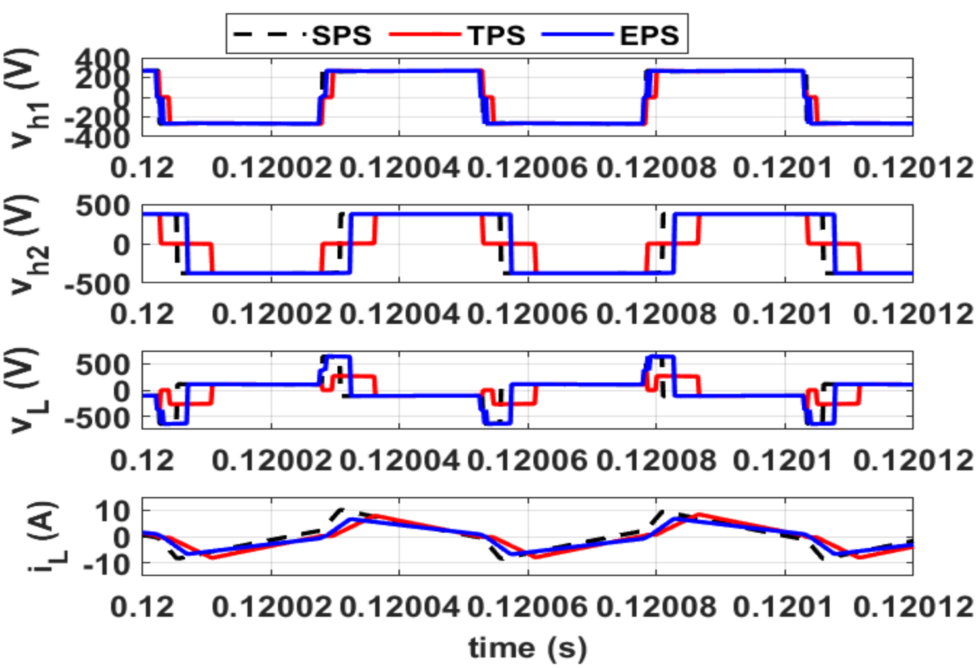

Fig. 6. Simulation results at V_{in} = 45 V, V_o = 375 V, P_o = 1 kW, and f = 20 kHz.

Hardware Results

Fig. 7 shows the hardware setup of the dual active bridge (DAB) converter. Transformer designs corresponding to two different operating frequencies—20 kHz and 50 kHz—are illustrated in Fig. 8. The hardware results for DAB with SPS control are shown in Fig. 9 for two different power levels (500 W and 900 W). The measured thermal images at steady state are shown in Fig. 10 for transformer and input side-H bridge.

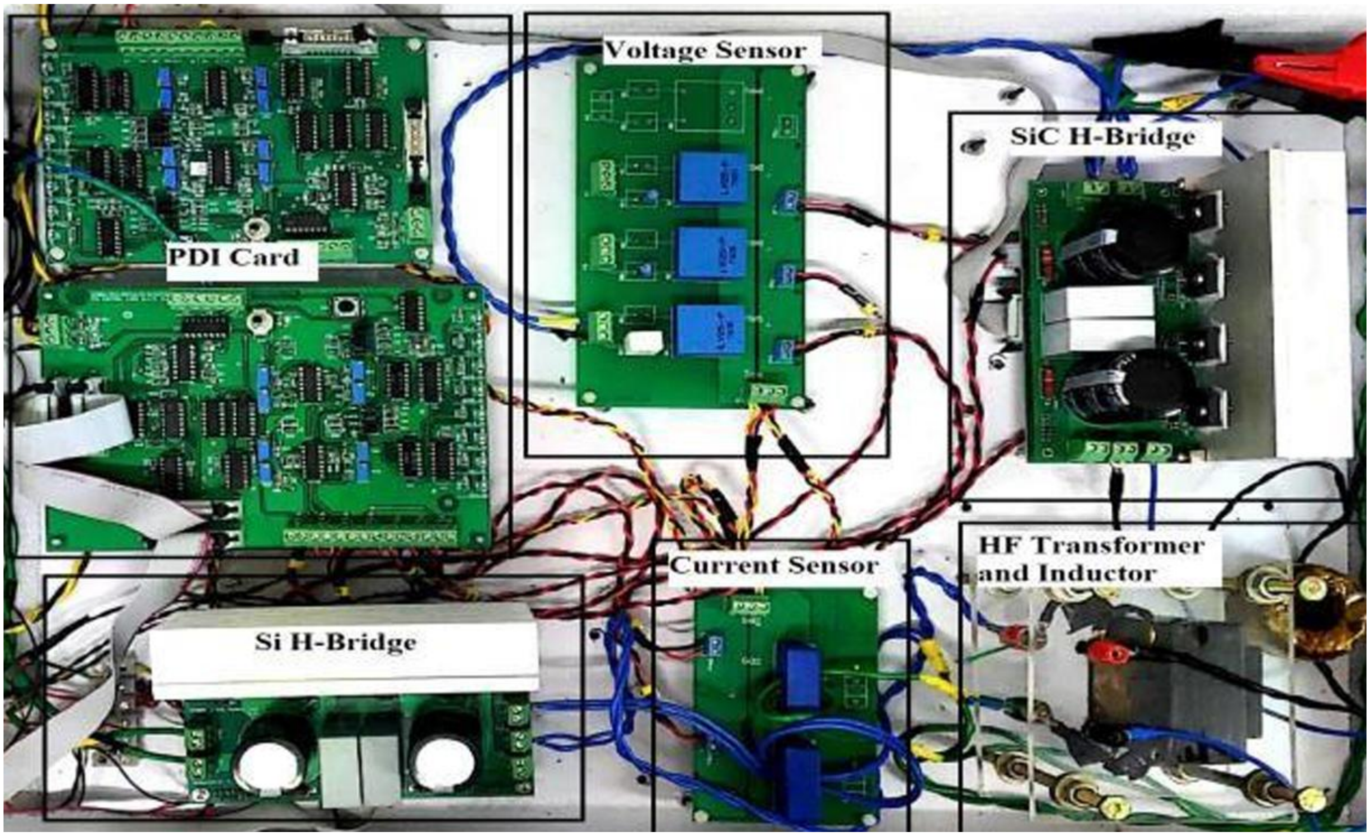

Fig. 7. Hardware setup of DAB.

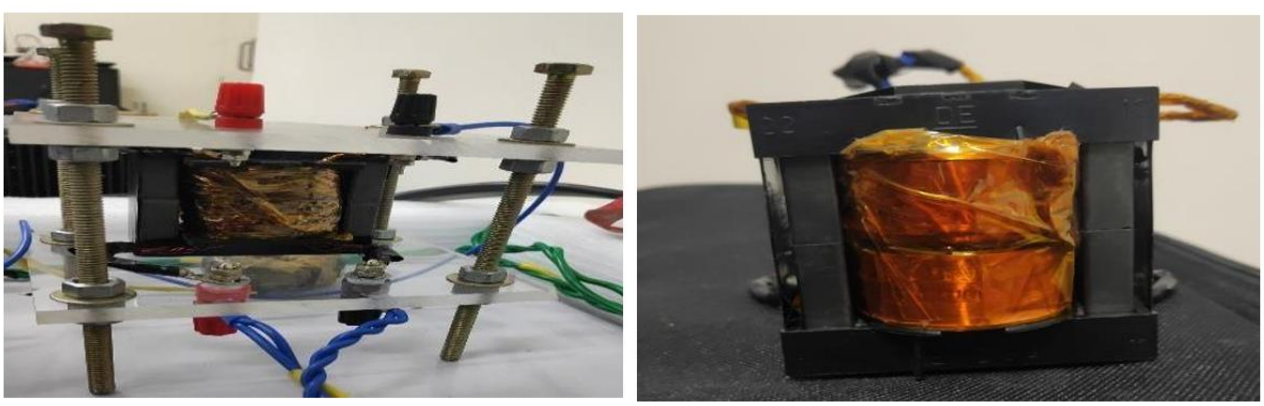

Fig. 8. High-frequency transformer prototype: 20 kHz (left) and 50 kHz (right).

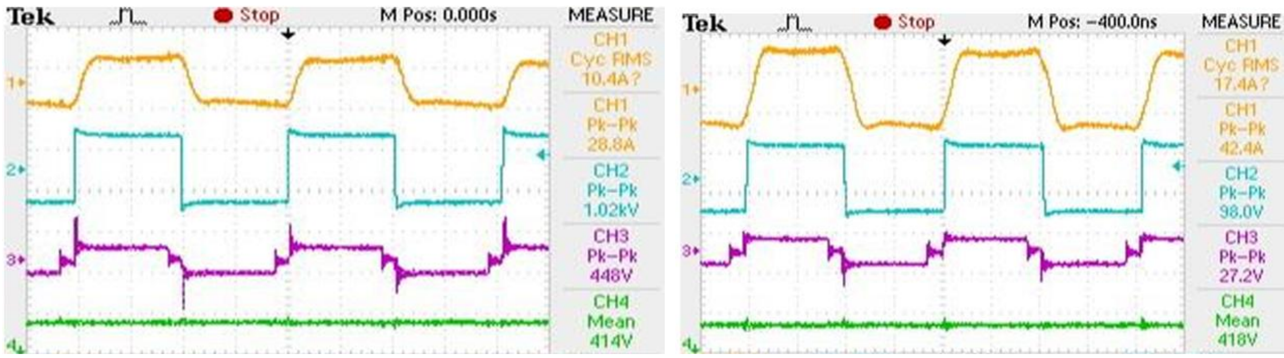

(a) (b)

Fig. 9. Waveforms for DAB operating at P_o = 500 W (a) and P_o = 900 W (b). Scope settings are ch1: 20 A/div, ch2: 500 V/div, ch3: 200 V/div, ch4: 500 V/div, and time: 10 μs/div.

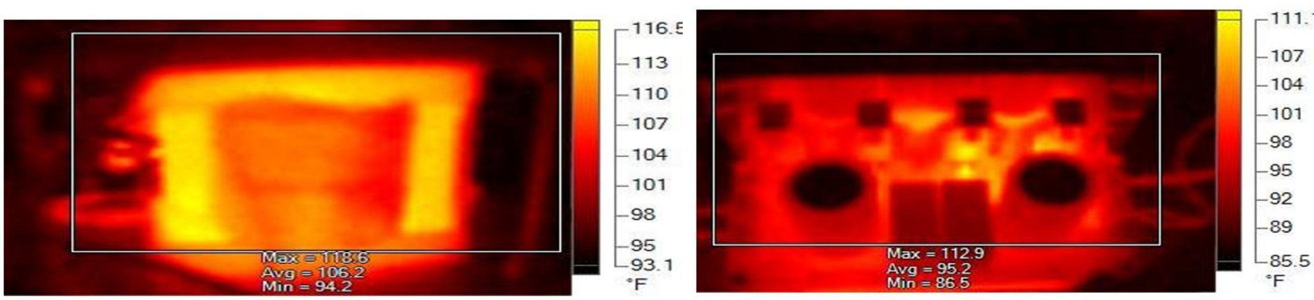

Fig. 10. Thermal images with 900-W loading with the transformer (left) and input side H-bridge (right) shown.

Conclusion

In this article, effective bidirectional power converter configurations were studied for electric vehicles. It was determined that dual active bridge is one of the promising topological configurations in this regard. The basic operating principles were discussed and converter modulation techniques were evaluated with regard to their effect on the efficiency and magnetic component selection.

As was observed, different choices of operating frequency and different selections of devices can affect the efficiency and magnetic design significantly. The efficiency of the DAB converter improves by 3% with TPS control and by 3.65% with EPS control, compared to SPS control. The area product of the magnetic components in the DAB converter is reduced by 26% with TPS control and by 36.3% with EPS control, relative to SPS control. This reduction directly translates to smaller transformer and inductor requirements. The concept can be extended to replace multiple dc-dc converters with a multiport converter.

Acknowledgments

This work is supported by ANRF, Department of Science and Technology, India [ANRF File No: CRG/2022/000650].

References

1. "Global EV Outlook 2025," annual report published by International Energy Agency (IEA), May 14, 2025.
2. "An engineer's guide to the DC power train architecture of an electric vehicle," by Dermot Byrne, Director Industry Marketing, Transportation, TTI Europe.
3. EV Publication Final Report.

4. "ELECTRIC VEHICLE INCENTIVES," e-AMRIT (Accelerated e-Mobility Revolution for India's Transportation) portal.
5. "High-Frequency-Linked Three-Port Converter with Optimized Control Strategies Based on Power System Load Flow Concepts for PV-Battery Systems" by Md. Mejbaul Haque, Peter J. Wolfs, Sanath Alahakoon, and Frede Blaabjerg, IEEE Journal of Emerging and Selected Topics in Power Electronics, vol. 10, no. 1, pp. 1032-1045, 2022.
6. "A three-phase soft-switched high-power-density DC/DC converter for high-power applications" by R. W. A. A. De Doncker, D. M. Divan and M. H. Kheraluwala, IEEE Transactions on Industry Applications, vol. 27, no. 1, pp. 63-73, Jan.-Feb. 1991.
7. "Performance characterization of a high-power dual active bridge DC-to-DC converter" by M. N. Kheraluwala, R. W. Gascoigne, D. M. Divan and E. D. Baumann, IEEE Transactions on Industry Applications, vol. 28, no. 6, pp. 1294-1301, Nov.-Dec. 1992.
8. "Minimum-Current-Stress Scheme of Dual Active Bridge DC–DC Converter With Unified Phase-Shift Control" by Nie Hou, Wensheng Song and Mingyi Wu, IEEE Transactions on Power Electronics, vol. 31, no. 12, pp. 8552-8561, Dec. 2016.
9. "Current Stress Minimization of Dual-Active-Bridge DC–DC Converter Within the Whole Operating Range" by Qing Gu, Liqiang Yuan, Jintong Nie, Jianning Sun and Zhengming Zhao, IEEE Journal of Emerging and Selected Topics in Power Electronics, vol. 7, no. 1, pp. 129-142, March 2019.
10. "Minimum Backflow Power and ZVS Design for Dual-Active-Bridge DC–DC Converters" by Fei Xu, Junwei Liu and Zheng Dong, IEEE Transactions on Industrial Electronics, vol. 70, no. 1, pp. 474-484, Jan. 2023.
11. "Study of Dual Active Bridge with Modified Modulation Techniques for Harmonic Reduction in AC Link Current" by Srija Mukherjee, Abinash Dash, Dipankar De and Alberto Castellazzi, 2019 IEEE International Conference on Sustainable Energy Technologies and Systems (ICSETS), Bhubaneswar, India, 2019, pp. 144-149.
12. "Design and comparison of high frequency transformers using foil and round windings," by K. V. Iyer, W. P. Robbins and N. Mohan, 2014 IPEC Hiroshima 2014 – ECCE ASIA, Hiroshima, Japan, pp. 3037-3043.
13. *Power Electronics: Converters, Applications, and Design, Third Edition,* by N. Mohan, T. M. Undeland, and W. P. Robbins, Wiley, 2002.

About The Authors

Silpashree Sahu is currently working toward the Ph.D. degree in power electronics with the School of Electrical and Computer Sciences, Indian Institute of Technology, Bhubaneswar, India. From 2017 to 2021, she was an assistant professor at the School of Electrical Engineering, Kalinga Institute of Industrial Technology (KIIT), Bhubaneswar, India. Her research interests include dc-dc converters, power electronics in renewable energy systems, and control systems. Sahu received the B.Tech. degree in electrical engineering from the College of Engineering and Technology, Bhubaneswar, India and the M.Tech. degree in electric drives and power electronics from the Indian Institute of Technology, Roorkee, India. She can be reached at s22ee09002@iitbbs.ac.in.

Abinash Dash has worked as JRF with the Department of Electrical Engineering, Indian Institute of Technology Bhubaneswar, Bhubaneswar, India from 2017 to 2021. His research interests include analysis and control design of high-frequency dc–dc converters and magnetics. Dash received the B.Tech. degree in electrical and electronics engineering from the Biju Patnaik University of Technology, Rourkela, India and the M.Tech. degree in power electronics control and drives from the Veer Surendra Sai University of Technology, Sambalpur, India. He can be reached at abinash.dash2013@gmail.com

Dipankar De is currently an associate professor with the School of Electrical Sciences, Indian Institute of Technology Bhubaneswar, Bhubaneswar, India. From 2011 to 2014, he was with the University of Nottingham, Nottingham, U.K., where he was involved in the development of efficient energy storage systems and compact power converter design with wide-bandgap semiconductors. From 2014 to 2016, De was with Ryerson University, Toronto, ON, Canada, as a research fellow and worked for a sponsored project funded by Rockwell Automation, Cambridge, ON, Canada. His research interests include power electronics converter systems for renewable energy, power quality, and electric vehicles applications. De received the Ph.D. degree in power electronics from the Indian Institute of Science, Bangalore, India. He can be reached at dipankar@iitbbs.ac.in.

Harikrishnan A is currently working in Bharat Petroleum. From May through June 2025, he was employed and contributed towards the ANRF-sponsored project "Optimized Modulation of Triple Active Bridge Converter for Electric Vehicle Application with Wide Band Gap Semiconductor Devices" at IIT Bhubaneswar. His academic interests lie in optimization of performance and magnetic design of the dual active bridge converter. Harikrishnan A completed his B.Tech in electrical engineering from the Indian Institute of Technology Bhubaneswar, India. He can be reached at 21ee01013@iitbbs.ac.in.

Varri Chandra Sekhar Pavan Kumar has worked as a junior research fellow at IIT Bhubaneswar on power electronic converters for electric vehicle applications. He has also interned at Purewatt Renewables and APGENCO. His academic interests lie in power electronics, control systems, sustainable technologies. Kumar completed his B.Tech in electrical and electronics engineering from JNTUA, Andhra Pradesh, India. He can be reached at vcpk10@iitbbs.ac.in.

Alberto Castellazzi leads research and teaching in advanced solid-state power processing, with a focus on wide-bandgap semiconductor devices, their packaging and thermal management, to yield disruptive joint progress in efficiency, power density and reliability of power converters. He has been involved in power electronics R&D for over 25 years, published over 300 papers in international journals and conference proceedings and held a number of invited talks, tutorials and seminars on the topic of WBG power devices and their application. He can be reached at alberto.castellazzi@kuas.ac.jp.

For further reading on designing dc-dc converters, see the How2Power Design Guide, locate the "Power Supply Function" category and select "DC-DC converters".